Front. Optoelectron. 2016, 9(3): 428–435
DOI 10.1007/s12200-016-0591-6

RESEARCH ARTICLE

Cross-cascaded AWG-based wavelength selective switching integrated module using polymer optical waveguide circuits

Changming CHEN, Daming ZHANG (✉)

State Key Laboratory on Integrated Optoelectronics, College of Electronic Science and Engineering, Jilin University, Changchun 130012, China

Abstract 100-GHz cross-cascaded arrayed waveguide gratings (AWGs)-based wavelength selective optical switching optical cross-connects (OXCs) modules with Mach-Zehnder interferometer (MZI) thermo-optic (TO) variable optical attenuator (VOA) arrays and optical true-time-delay (TTD) line arrays is successfully designed and fabricated using polymer photonic lightwave circuit. Highly fluorinated photopolymer and grafting modified organic-inorganic hybrid material were synthesized as the waveguide core and cladding, respectively. The one-chip transmission loss is ~6 dB and the crosstalk is less than ~30 dB for the transverse-magnetic (TM) mode. The actual maximum modulation depths of different thermo-optic switches are similar, ~15.5 dB with 1.9 V bias. The maximum power consumption of a single switch is less than 10 mW. The delay time basic increments are measured from 140 to 20 ps. Proposed novel module is flexible and scalable for the dense wavelength division multiplexing network.

Keywords polymer waveguides, photosensitive materials, integrated optics devices, photonics integrated circuits

1 Introduction

Wavelength routing optical path networks employing reconfigurable optical add/drop multiplexers (ROADMs) or optical cross-connects (OXCs) are being deployed widely throughout the world to cope with the rapid traffic expansion spurred by the penetration of broadband access services including asymmetric digital subscriber line (ADSL) and fiber to the home (FTTH) [1–4]. Most existing ROADM/OXC systems are developed on wavelength selective switches (WSSs) [5–7]. To realize the optical network, several technologies have been adopted to build the OXC module, including hybrid fiber Bragg gratings (FBGs) with optical circulators (OCs) [8–10] as well as variable optical attenuator (VOA) array associated with optical switches (OSWs) [11,12]. The latest ROADM recently reported is based on $N \times N$ arrayed waveguide grating (AWG) integrated with OSWs arrays to carry out the add-drop function [13–16]. Several material systems [17–24] have been used to fabricate the ROADM modules, the notable being lithium niobate, silicon-on-insulator (SOI), InP and polymers. As a multifunctional material system, polymers exhibit well-controlled refractive indices, highly flexible structures, and large thermo-optic (TO) and electro-optic (EO) coefficients [25–30], which can be advantageous to reduce manufacturing costs and open possibility of monolithic integration with functional devices such as lasers and detectors.

To deal with this traffic increase more efficiently in optical networks, it is necessary to give a network the flexibility of actively reconfiguring the signal path of various traffic loads in a remote node from the central office. This flexibility of reconfiguring network nodes is essential for the evolution of an existing network into an intellectual optical network, and an ROADM module is the most important device for this purpose.

In this paper, we proposed a novel monolithically integrated OXC module comprised of double 16-channel 100-GHz cross-cascaded AWG-based wavelength selective optical switches using polymer photonic lightwave circuit. Fluorinated polycarbonate negative-type photopolymer and grafting modified organic-inorganic hybrid materials were synthesized as the waveguide core and cladding, respectively. Cross-cascaded AWG-based wavelength selective switching, VOA-arrayed and true-time-delay (TTD) arrayed characteristics were analyzed, simulated and measured. The fabrication process of the integrated OXC chip was described. Optimized structural properties of waveguides and electrode heaters were shown. Through careful design and fabrication of the integrated OXC chip, the excellent performances of the

Received December 31, 2015; accepted June 15, 2016

E-mail: zhangdm@jlu.edu.cn

module were achieved. The cross-cascaded integrated module with double 100-GHz AWG-based wavelength selective optical switches the integrated module can manipulate the multiplexed channel signal wavelengths to realize the add-drop function more flexibility. Moreover, the output wavelength spacing for the same channel can be controlled as integer multiple of $\Delta\lambda$ more freely. The selective switching characteristics between 16 channels can achieve greater extent in the use of the network wavelength resources.

2 Design and experiments

2.1 Device structure

Based on our monolithic multi-functional waveguide chip [31,32], novel polymer monolithically integrated reconfigurable OXC module was designed and fabricated. The schematic configuration of the integrated OXC module are shown in Fig. 1.

Wavelength assignment relation of AWG can be given as described in Ref. [33].

$$\lambda_{i+N} = \lambda_i + FSR = \lambda_i + N\Delta\lambda, \tag{1}$$

$$\lambda_{i\to j} = \lambda = \lambda_0 + (i+j)\Delta\lambda, \tag{2}$$

where λ_0 is the central wavelength, FSR is the free spectral range, $\Delta\lambda$ is the wavelength spacing, N is the channel number, and λ_i *is* the wavelength from *i*th channel.

The metal electrodes of the serpentine heaters are set on the arrayed waveguides region of the AWG. The length difference between the adjacent electrodes is ΔL_e. The adjacent electrodes are connected to each other end to end. The functional AWG device is based on the grating equation as the following [34].

$$\frac{\Delta\phi - 2\pi m}{2\pi n_s d/\lambda} = \theta, \tag{3}$$

where n_s is the effective index of the slab region, m is the diffraction order of the array, d is the arrayed waveguides separation and λ is the wavelength of the incident beam. Equation (3) shows that dispersion angle θ is resulting from a phase difference between adjacent waveguides $\Delta\phi$. However, if the temperature of the waveguides shifts $j\Delta T$ ($j = 0,\pm1,\pm2,\ldots$) owing to the electrodes, the refractive

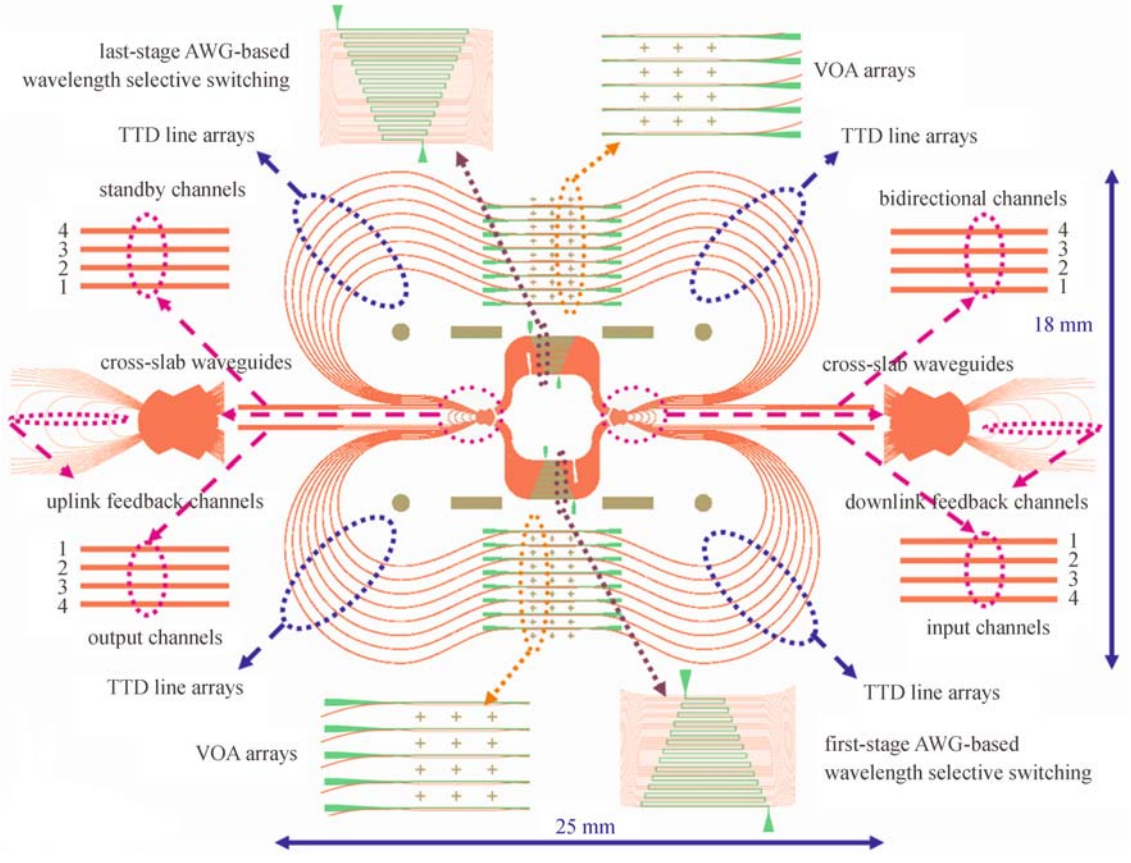

Fig. 1 Schematic configuration of integrated OXC module

index of the arrayed waveguides with change $j\Delta n_c$, $\Delta\phi$ is determined by two compositions

$$\Delta\phi = \frac{2\pi}{\lambda}(n_c\Delta L + j\Delta n_c\Delta L_e). \quad (4)$$

The relations can be written as

$$\frac{j\Delta x}{j\Delta n_c} = \frac{R\Delta L}{n_s d}, \quad (5)$$

where Δx is the output waveguides separation, and R is the focal length. The variation of the focal position x will depend on the index migration Δn_c. When the thermal shift from $(T_0 - j\Delta T)$ to $(T_0 + j\Delta T)$, the beam will export from channel $-j$ to channel j. Then the wavelength-channel-selective function is realized.

2.2 Analysis and simulation

To ensure the low-loss single-mode polymer optical waveguide for planar lightwave circuits (PLCs), negative-type fluorinated photoresist and organic-inorganic grafting polymethylmethacrylate (PMMA) were used as the waveguide core and cladding, respectively. Highly fluorinated polystyrene derivates (FPSDs) [35] were synthesized by copolymerization of 2,3,4,5,6-pentafluorostyrene (PFS) and fluorinated styrene derivate monomer (FSDM). The fluorinated polymers were doped into epoxy SU-8 resist using diphenyl iodonium salt as a photoacid generator (PAG). The refractive index and crosslinking density of the negative-type fluorinated photoresists can be tuned and controlled by monitoring the feed ratio of comonomers. The SiO_2-TiO_2 network grafting PMMA material [36] offers some advantages such as low birefringence, good thermal stability and low wavelength dispersion. The refractive index of the sol-gels can be adjusted by monitoring the composition of TiO_2 in hybrid materials. The refractive indices (n) of the polymeric core and cladding materials measured with an M-2000UI variable angle incidence spectroscopic ellipsometer are 1.571 and 1.560 at 1550-nm wavelength, respectively. The relative refractive index difference between the core and the cladding is about $\Delta = (n_1 - n_2)/n_1 = 0.7\%$. The relations based on the eigenvalue equations [37] between the core thickness b and mode effective refractive indices n_c and n_s of the slab and the arrayed waveguides for the signal wavelength are shown in Fig. 2. The eigenvalue equations [37] are established through the parts of the slab and arrayed waveguides for the signal wavelength.

Figure 3 shows the transverse-magnetic (TM) mode spectral response of the integrated ROADM module. There are 16 peaks in the spectra, obtained at the through port and each of the seven drop ports. One is the through signal, including λ_8 which only passes through the demultiplexer, and $\lambda_9 - \lambda_{16}$ modulated signals which pass through the demultiplexer, TTD lines, thermo-optic switch, and multiplexer. The others ($\lambda_1 - \lambda_7$) are the drop signals. The one-chip transmission loss is ~6 dB and the crosstalk is less than ~30 dB for the transverse electric mode.

Figure 4 shows the simulation results at different temperature of the serpentine heaters for wavelength-channel-selected function. When the input wavelength λ_1 is 1544.4 nm, the insertion loss of this AWG component is below ~5.37 dB, and the extinction ratio is better than ~31 dB. As temperature changes from 20°C to 65°C, we can observe that when the temperature is increased by 3°C, the signal wavelength can be transferred to the next channel. Heat-driven power of electrodes is about 5.2 mW/channel based on the three-layer active region's temperature distributions by Fourier transform method [38].

2.3 Fabrication procedure

The fabrication process is shown in Fig. 5. It shows that the organic-inorganic hybrid thin film with the thickness of 10

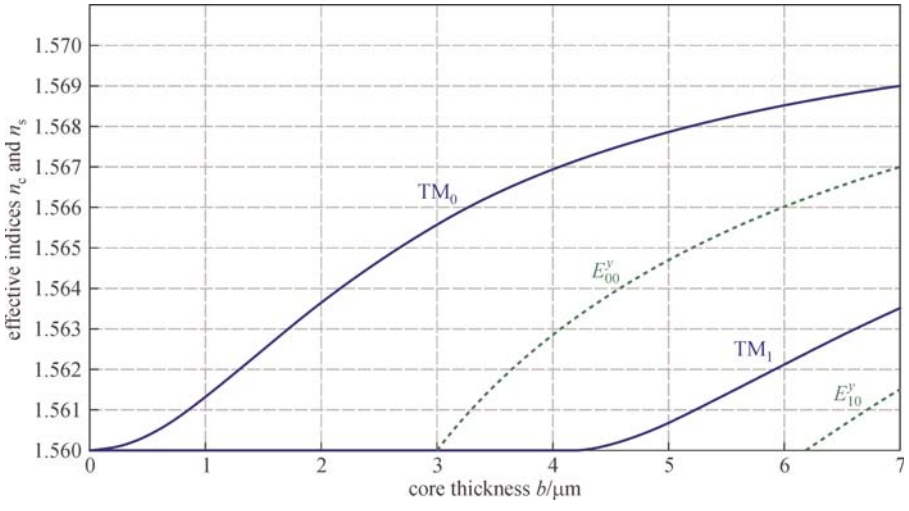

Fig. 2 Relations between the core thickness b and the effective refractive indices n_c (green dashed lines) and n_s (blue solid lines) with $a = b$

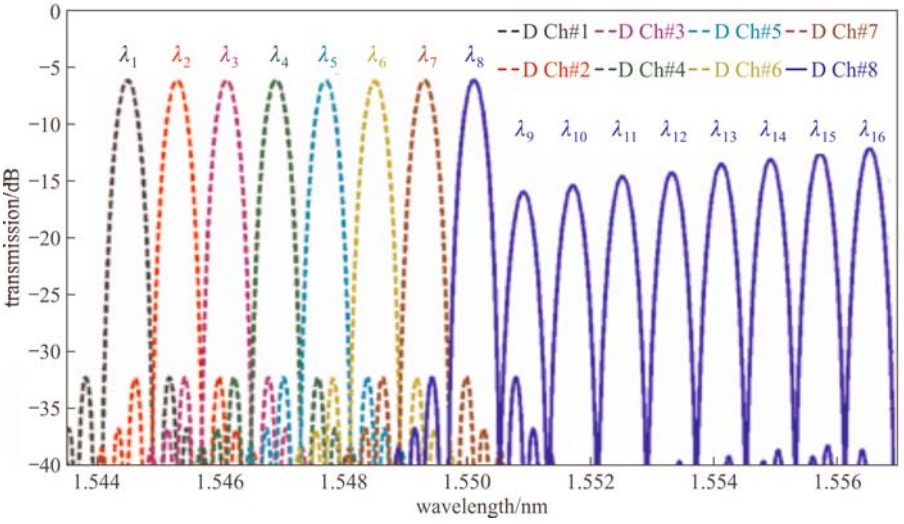

Fig. 3 Output spectra of transmitted signal lights for each channel

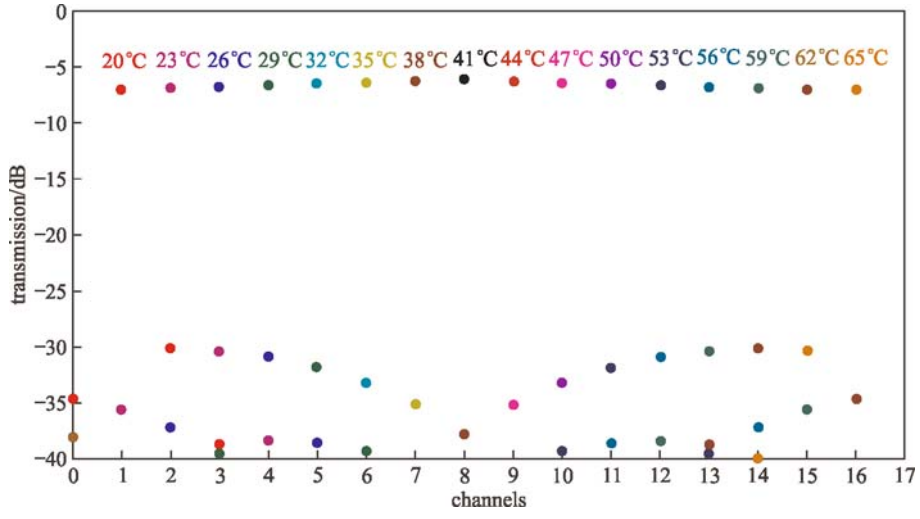

Fig. 4 Simulated output wavelength-channel-selected characteristics of the integrated module with temperature ranging from 20°C to 65°C

μm was formed as the cladding layer by spin coating on Si substrate, and the wafer was done by thermal annealing at 125°C for 1 h to cross-link the polymer as the bottom layer. The layer thickness of 10 μm is sufficient to reduce the optical leakage into the substrate. A fluorinated SU-8 photoresist with the thickness of 4 μm was spin-coated on the bottom cladding as waveguide layer, and then pre-baked at 65°C for 10 min and 90°C for 20 min to remove any traces of the solvent. The pattern exposure was performed at a wavelength of 365 nm using a 350 mW mercury lamp through a contact chromium mask. The exposure time was 180 s. After post-baking, the resist was developed in propylene glycol-monomethyl ether-acetate (PGMEA) for 40 s, rinsed in isopropyl alcohol and then deionized water, and blew dry to form the channel waveguides. After that, it is very important to curing-bake the wafer at 150°C for 30 min so that the adhesion between polymeric waveguides and bottom cladding layer can be enhanced well. A 10-μm-thick organic-inorganic hybrid film was spin-coated as the upper cladding layer to further reduce the optical leakage from waveguides into the metal film. Finally, the aluminum electrode heaters were patterned by photolithography and wet etching.

Scanning electron microscope (SEM) micrographs of the cross sections of the input waveguide are shown in Fig. 6(a). It indicates the cross section of the waveguide by SEM. It shows that the ridge-wall is smooth and almost vertical. Figure 6(b) gives structural patterns of the electrode heaters from TO VOA arrays by microscope (×1000). The value of the resistance is about 200 Ω. Figure 6(c) gives interactional segments patterns of the serpentine electrode heaters by microscope (×1000). It

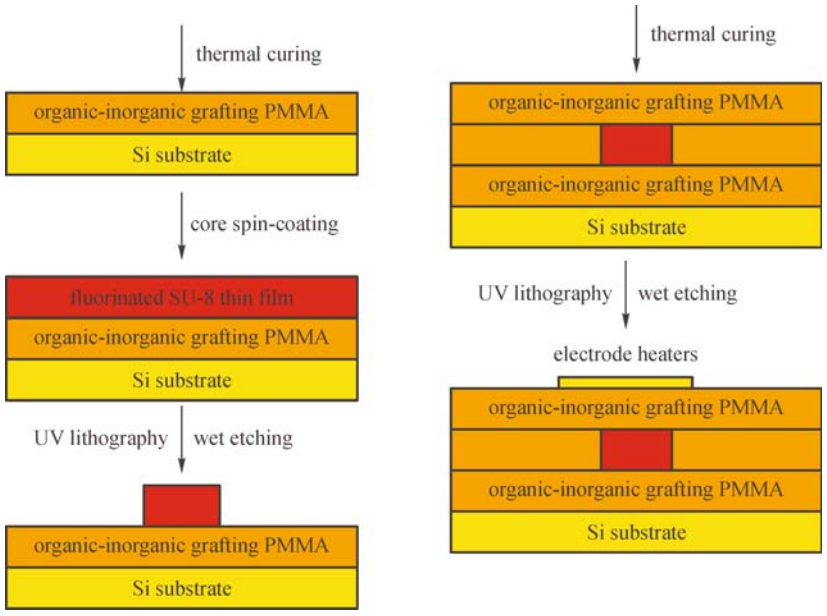

Fig. 5 Fabrication process for UV defined waveguide and electrode heater structure

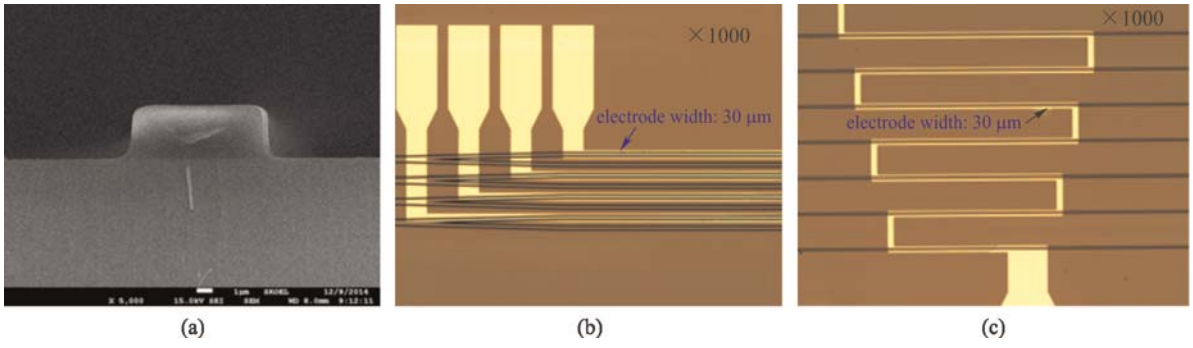

Fig. 6 (a) Scanning electron microscope (SEM) photographs of transmission segment patterns of cross-sectional waveguides; the surface profiles of (b) thermo-optic (TO) variable optical attenuator (VOA) arrayed and serpentine electrode heater (c)

shows that the parameters designed of the serpentine electrode heaters can be realized very well. The measured total resistance was 500 Ω.

3 Results and discussion

The propagation loss of a 4-μm-wide straight waveguide, measured by a cutback method at 1550 nm, was found to be 0.15 dB/cm. Schematic photographs of the proposed polymer multi-functional integrated OXC module measured were shown in Fig. 7(a). Figure 7(b) gives the near-field patterns of the device. Signal light from a wide-band erbium-doped optical fiber amplifier (EDFA) was butt-coupled into the input waveguide through standard single-mode fiber. The signals from the output waveguides were magnified (×60) by lens and received by the CCD camera. The channel spacing was 0.795 nm/channel, the fiber–fiber insertion loss at each channel was ranged from 5.52 to 6.43 dB, and the crosstalk of the 16 channels was about −20 dB.

Figure 8 shows the actual spectral response of the integrated OXC module based on the last-stage AWG-based WSS functions with TO tuning effect. The straight-through transmission loss of the integrated module was about 5.5 dB and the crosstalk was less than ~20 dB for the TM mode. As shown in Fig. 8(a), it was indicated that when the driving voltage of the serpentine electrode heaters was 0 V, the actual spectral response was from the output channels and bidirectional channel#0. The actual spectrum in Fig. 8(b) was shown that when the driving voltage was applied as 1.5 V and heat-driven power of electrodes was about 5.5 mW/channel, signals of λ_{-4}~λ_{-7} can be adjusted into modulation channel#1 by uplink feedback channels, then demultiplexed into downlink feedback channels and multiplexed into the output channel#0. The maximum attenuation depth of the modulation channels was ~15 dB under a bias of 2.5 V. The maximum power consumption of a single TO VOA was about 8 mW. For the TTD line arrays of the modulation channels, the delay length increments were

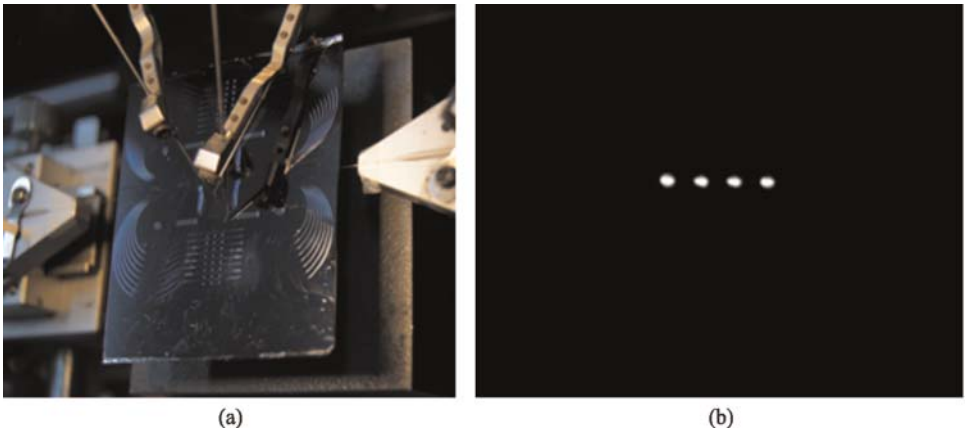

Fig. 7 (a) Schematic photographs of the proposed polymer integrated optical cross-connects (OXCs) module measured; (b) near-field guide-mode patterns of the device with signal light from a wide-band erbium-doped optical fiber amplifier (EDFA)

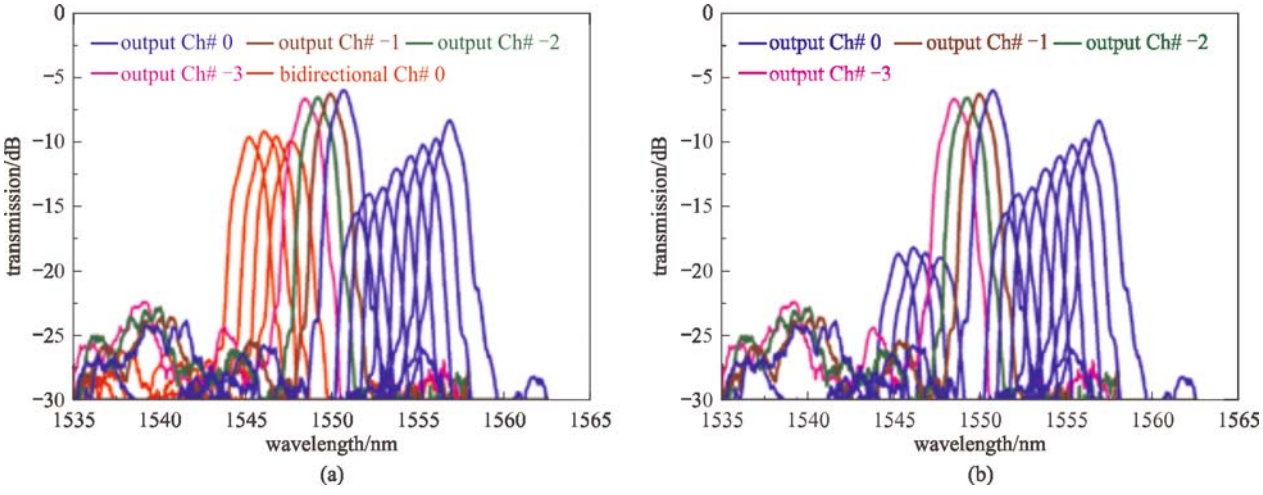

Fig. 8 Actual output spectral response from the output channels (a) when driven voltage is 0 V for the last-stage AWG-based wavelength selective switches(WSS); (b) when the λ_{-4}~λ_{-7} were directly multiplexed into 1st to 8th modulation channels

selected to decrease from the channel #1 to #8 by 3.8 mm, corresponding to 20 ps in time delay. The basic physical delays were 455 ps for the modulation channel#1, the maximum time-delay error was obtained less than 0.1 ps, corresponding to a radiation angle error of less than 0.5°, which was within the equipment resolution.

Figure 9(a) shows that the TO switching response is observed by applying square–wave voltage at a frequency of 100 Hz. It can be noted that the rise and fall times were 190 and 350 μs, respectively. Figure 9(b) gives that how channel output intensity was changing with power consumption of optical switch at 1550 nm for TM mode. The extinction ratio of the TO switch was measured about ~15.5 dB with 2.4 V bias. The applied electric power as the switching power was actually 9.5 mW.

4 Conclusion

In summary, 16-channel 100-GHz cross-cascaded AWG-based wavelength selective optical switches with 8-channel MZI TO VOA arrays and optical TTD line arrays were successfully designed and fabricated using polymer photonic lightwave circuit. Proper OXC function was confirmed through C-band spectral channels input. Utilizing the cyclic AWG-based WSS, the proposed OXC module allowed to handle all the wavelengths in the network channels freely. The preferable structural profiles of waveguide and electrode were obtained by SEM and optical microscope. These characteristics were advantageous to optimize producing process and enhance optical performances of polymer waveguide devices. The one-chip transmission loss was ~6 dB and the crosstalk was less than ~30 dB for the TM mode. The actual maximum modulation depths of different TO switches were similar, ~15.5 dB with 1.9 V bias. The maximum power consumption of a single switch was less than 10 mW. The basic increments of delay time varied from 140 to 20 ps. The technique is very useful for efficient dense

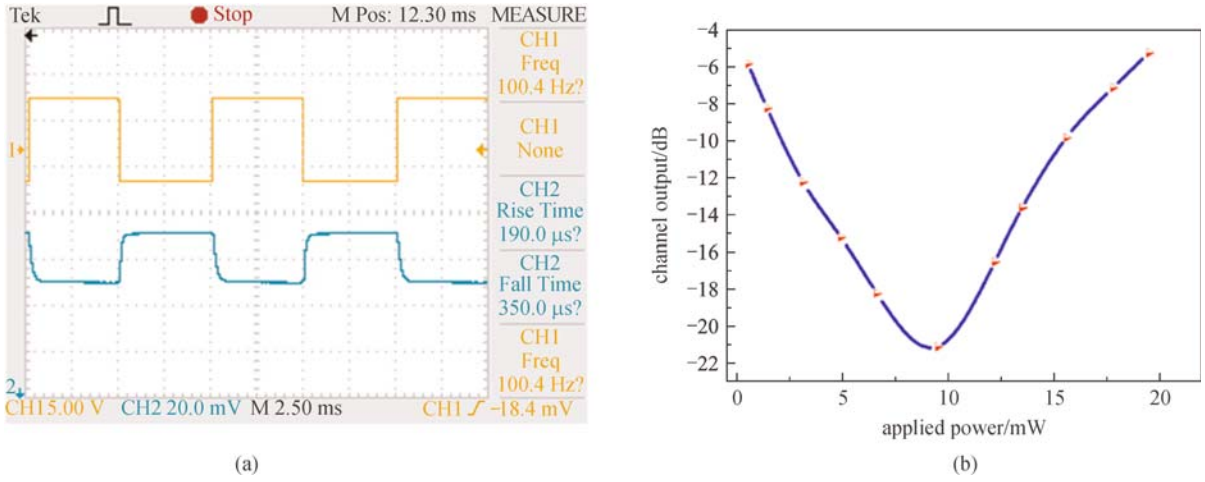

Fig. 9 Performances of integrated device. (a) TO switch responses obtained by applying square-wave voltage at frequency of 100 Hz; (b) actual channel output versus power consumption of optical switch at 1550 nm for TM mode

wavelength division multiplexing (DWDM) optical communication systems and large-scale photonics integrated circuits.

Acknowledgements The authors gratefully acknowledged financial support from the National Natural Science Foundation of China (Grant Nos. 61261130586,61275033 and 61205032), Science and Technology Development Plan of Jilin Province (Nos. 20130522151JH and 20140519006JH).

References

1. Zami T. Current and future flexible wavelength routing cross-connects. Bell Labs Technical Journal, 2013, 18(3): 22–38
2. Iwai Y, Hasegawa H, Sato K. A large-scale photonic node architecture that utilizes interconnected OXC subsystems. Optics Express, 2013, 21(1): 478–487
3. Sato K, Hasegawa H. Optical networking technologies that will create future bandwidth-abundant networks. Journal of Optical Communications and Networking, 2009, 1(2): A81–A93
4. Le H C, Hasegawa H, Sato K. Performance evaluation of large-scale multi-stage hetero-granular optical cross-connects. Optics Express, 2014, 22(3): 3157–3168
5. Li Z, Claver H. Compact wavelength-selective optical switch based on digital optical phase conjugation. Optics Letters, 2013, 38(22): 4789–4792
6. Rohit A, Bolk J, Leijtens X J M, Williams K A. Monolithic nanosecond-reconfigurable 4×4 space and wavelength selective cross-connect. IEEE Journal of Lightwave Technology, 2012, 30 (17): 2913–2921
7. Stabile R, Rohit A, Williams K A. Monolithically integrated 8×8 space and wavelength selective cross-connect. IEEE Journal of Lightwave Technology, 2014, 32(2): 201–207
8. Tran V, Zhong W D, Tucker R S, Song K. Reconfigurable multichannel optical add–drop multiplexers incorporating eight-port optical circulators and fibre Bragg gratings. IEEE Photonics Technology Letters, 2001, 13(13): 1100–1102
9. Han Y T, Shin J U, Park S H, Seo J K, Lee H J, Hwang W Y, Park H H, Baek Y. 2×2 polymer thermo-optic digital optical switch using total-internal-reflection in bend-free waveguides. IEEE Photonics Technology Letters, 2012, 24(19): 1757–1760
10. Claes T, Bogaerts W, Bienstman P. Vernier-cascade label-free biosensor with integrated arrayed waveguide grating for wavelength interrogation with low-cost broadband source. Optics Letters, 2011, 36(17): 3320–3322
11. Han Y, Shin J, Park S, Han S, Baek Y, Lee C, Noh Y, Lee H, Park H. Fabrication of 10-channel polymer thermo-optic digital optical switch array. IEEE Photonics Technology Letters, 2009, 21(20): 1556–1558
12. Segawa T, Matsuo S, Kakitsuka T, Shibata Y, Sato T, Kawaguchi Y, Kondo Y, Takahashi R. All-optical wavelength-routing switch with monolithically integrated filter-free tunable wavelength converters and an AWG. Optics Express, 2010, 18(5): 4340–4345
13. Fang Q, Song J, Zhang G. Monolithic integration of a multiplexer/demultiplexer with a thermo-optic VOA array on an SOI platform. IEEE Photonics Technology Letters, 2009, 21(5): 319–321
14. Yeniay A, Gao R. True time delay photonic circuit based on perfluorpolymer waveguides. IEEE Photonics Technology Letters, 2010, 22(21): 1565–1567
15. Oguma M, Kamei S, Kitoh T, Hashimoto T, Sakamaki Y, Itoh M, Takahashi H. Wide passband tandem MZI-synchronized AWG empolying mode converter and multimode waveguide. IEICE Electronics Express, 2010, 7(11): 823–826
16. Segawa T, Matsuo S, Kakitsuka T, Shibata Y, Sato T, Kawaguchi Y, Kondo Y, Takahashi R. All-optical wavelength-routing switch with monolithically integrated filter-free tunable wavelength converters and an AWG. Optics Express, 2010, 18(5): 4340–4345
17. Dai D, Bauter. J, Bowers J E. Passive technologies for future large-scale photonic integrated circuits on silicon: polarization handling, light non-re1ciprocity and loss reduction. Light, Science & Applications, 2012, 1: e1
18. Bontempi F, Faralli S, Contestabile G. An InP monolithically integrated unicast and multicast wavelength converter. IEEE

Photonics Technology Letters, 2013, 25(22): 2178–2181
19. Andriolli N, Faralli S, Bontempi F, Contestabile G. A wavelength-preserving photonic integrated regenerator for NRZ and RZ signals. Optics Express, 2013, 21(18): 20649–20655
20. Andriolli, N, Faralli, S, and Leijtens, XJM. Monolithically integrated all-optical regenerator for constant envelope WDM signals. IEEE Journal of Lightwave Technology, 2013 31(2): 322–327
21. Francesca B, Sergio P, Nicola A. Multifunctional current-controlled InP photonic integrated delay interferometer. IEEE Journal of Quantum Electronics, 2012, 48(11): 1453–1461
22. Nicholes S C, Masanovic M L, Jevremovic B, Lively E, Coldren L A. An 8×8 InP monolithic tunable optical router (motor) packet forwarding chip. IEEE Journal of Lightwave Technology, 2010, 28: 641–650
23. Welch D F, Kish F A, Melle S, Nagarajan R, Kato M, Joyner C H, Pleumeekers J L, Schneider R P, Back J, Dentai A G, Dominic V G, Evans P W, Kauffman M, Lambert D J H, Hurtt S K, Mathur A, Mitchell M L, Missey M, Murthy S, Nilsson A C, Salvatore R A, Van Leeuwen M F, Webjorn J, Ziari M, Grubb S G, Perkins D, Reffle M, Mehuys D G. Large-scale InP photonic integrated circuits: enabling efficient scaling of optical transport networks. IEEE Journal of Selected Topics in Quantum Electronics, 2007, 13(1): 22–31
24. Wang J, Kroh M, Richter T, Theurer A, Matiss A, Zawadzki C, Zhang Z, Schubert C, Steffan A, Grote N, Keil N, Kroh M, Richter T. Hybrid-integrated polarization diverse coherent receiver based on polymer PLC. IEEE Photonics Technology Letters, 2012, 24(29): 1718–1721
25. Bamiedakis N, Beals J, Penty R V, White I H, DeGroot J V, Clapp T V. Cost-effective multimode polymer waveguides for high-speed on-board optical interconnects. IEEE Journal of Quantum Electronics, 2009, 45(4): 415–424
26. Gorman T, Haxha S, Ju J J. Ultra-high-speed deeply etched electrooptic polymer modulator with profiled cross section. IEEE Journal of Lightwave Technology, 2009, 27(1): 68–76
27. Chen C, Zhang F, Zhang D. UV curable electro-optic polymer switch based on direct photo definition technique. IEEE Journal of Quantum Electronics, 2011, 47(7): 959–964
28. Dalton L R, Sullivan P A, Bale D H. Electric field poled organic electro-optic materials: state of the art and future prospects. Chemical Reviews, 2010, 110(1): 25–55
29. Hassan K, Weeber J C, Markey L, Dereux A, Pitilakis A, Tsilipakos O, Kriezis E E. Thermo-optic plasmo-photonic mode interference switches based on dielectric loaded waveguides. Applied Physics Letters, 2011, 99(24): 241110
30. Chen C, Cui Z, Zhang D. Electro-optic modulator based on novel organic-inorganic hybrid nonlinear optical materials. IEEE Journal of Quantum Electronics, 2012, 48(1): 61–66
31. Chen C, Niu X, Han C, Shi Z, Wang X, Sun X, Wang F, Cui Z, Zhang D. Reconfigurable optical interleaver modules with tunable wavelength transfer matrix function using polymer photonics lightwave circuits. Optics Express, 2014, 22(17): 19895–19911
32. Chen C, Niu X, Han C, Shi Z, Wang X, Sun X, Wang F, Cui Z, Zhang D. Monolithic multi-functional integration of ROADM modules based on polymer photonic lightwave circuit. Optics Express, 2014, 22(9): 10716–10727
33. Oguchi K. New notations based on the wavelength transfer matrix for functional analysis of wavelength circuits and new WDM networks using AWG-based star coupler with asymmetric characteristics. IEEE Journal of Lightwave Technology, 1996, 14(6): 1255–1263
34. Hu G, Cui Y, Yun B, Lu C, Wang Z. A polymeric optical switch array based on arrayed waveguide grating structure. Optics Communications, 2007, 279(1): 79–82
35. Wan Y, Fei X, Shi Z, Hu J, Zhang X, Zhao L, Chen C, Cui Z, Zhang D. Highly fluorinated low-molecular-weight photoresists for optical waveguides. Journal of Polymer Science Part A, Polymer Chemistry, 2011, 49(3): 762–769
36. Chen C, Han C, Wang L, Zhang H, Sun X, Wang F, Zhang D. 650 nm all-polymer Thermo-optic waveguide switch arrays based on novel organic-inorganic grafting PMMA materials. IEEE Journal of Quantum Electronics, 2013, 49(5): 61–66
37. Kawano K. Introduction to Optical Waveguide Analysis: Solving Maxwell's Equations and the Schrödinger Equations. New York: Wiley, 2001
38. Hassan K, Weeber J C, Markey L, Dereux A, Pitilakis A, Tsilipakos O, Kriezis E E. Thermo-optic plasmo-photonic mode interference switches based on dielectric loaded waveguides. Applied Physics Letters, 2011, 99(24): 241110

Changming Chen received the B.S. degree in electronic science and technology, M.S. and Ph.D. degrees in microelectronics and solid electronics from Jilin University, Changchun, China, in 2005, 2007, and 2010, respectively. He has been a Faculty Member in Jilin University. His research interests include polymer integrated optical waveguide circuit devices (such as array waveguide grating multiplexers, electro-optic modulators and switches, ultra-long waveguide delay lines, and so on), and the second harmonic measuring systems for nonlinear optics.

Daming Zhang received the B.S., M.S. and Ph.D. degrees from the College of Electronic Science and Engineering, Jilin University, Changchun, China, in 1993, 1996, and 2000, respectively. Since 1996, he has been a Faculty Member in Jilin University. He has led more than 10 projects in the field of optical switching, high-speed lasers, polymer planar lightwave circuits (PLC), and wavelength division multiplexing systems. He has published more than 80 papers since 1999. He has been engaged in research and education on polymer photonics and PLC devices.

Prof. Zhang is currently the group leader of polymer PLC in the State Key Laboratory on Integrated Optoelectronics, Jilin University Region, Vice Dean in Collage of Electronic Science and Engineering, Jilin University, Changchun, China.